Nano Energy 66 (2019) 104184

Contents lists available at ScienceDirect

Nano Energy

journal homepage: http://www.elsevier.com/locate/nanoen

Full paper

Unveiling yavapaiite-type $K_xFe(SO_4)_2$ as a new Fe-based cathode with outstanding electrochemical performance for potassium-ion batteries

Wonseok Ko [a,1], Hyunyoung Park [a,1], Jae Hyeon Jo [a], Yongseok Lee [a], Jungmin Kang [a], Young Hwa Jung [b], Tae-Yeol Jeon [b], Seung-Taek Myung [a,**], Jongsoon Kim [a,*]

[a] Department of Nanotechnology and Advanced Materials Engineering, Sejong University, Seoul, 05006, Republic of Korea
[b] Beamline Division, Pohang Accelerator Laboratory (PAL), Pohang, 37673, Republic of Korea

ARTICLE INFO

Keywords:
$KFe(SO_4)_2$
First principle calculations
Intercalation
Cathode
Potassium
Battery

ABSTRACT

We report $KFe(SO_4)_2$ as a novel cathode material for potassium-ion batteries. The synthesis of phase-pure $KFe(SO_4)_2$ is confirmed through Rietveld refinement of X-ray diffraction data, and the ion diffusion path and possible positions of K^+ ions in the crystal structure are verified using bond-valence sum analysis. In addition, the theoretical average voltage, ion diffusion paths, and associated activation barrier energies obtained by first-principles calculations predict feasibility of the $KFe(SO_4)_2$ as a robust cathode for potassium-ion batteries. . Experimentally, the average working voltage of $KFe(SO_4)_2$ is approximately 3.3 V (*vs.* K^+/K) assisted by $Fe^{3+/2+}$ redox pair, and the resulting specific capacity (94 mAh g^{-1}) obtained at C/20 approaches to the theoretical capacity, 94 mAh g^{-1}. In addition, the capacity retention of $KFe(SO_4)_2$ at 2C was approximately 80% of the initial capacity after 300 cycles, with a Coulombic efficiency of over 99%. X-ray absorption near-edge structure and *operando* synchrotron X-ray diffraction analyses reveals the reversible change of the crystal structure with a minimal volume difference (1.83%) by occurrence of $Fe^{3+/2+}$ redox reaction during dis/charge. The demonstrated excellent structural stability of $KFe(SO_4)_2$ endorses feasibility of the $KFe(SO_4)_2$ as a sustainable cathode for potassium-ion batteries.

1. Introduction

The environmental impact of air pollutants such as fine dust particles like PM10 and PM2.5 (PM: particulate matter) originating from the use of fossil fuels is a major global issue, motivating considerable research interest in the efficient use and storage of eco-friendly and sustainable renewable energy systems [1–4]. Li-ion batteries (LIBs) are considered one of the most promising energy storage systems owing to their excellent electrochemical properties, including their high energy density, which is attributed to the high redox potential of Li^+/Li (−3.04 V *vs.* the standard hydrogen electrode (SHE)) [5–13]. However, the ongoing depletion of limited Li sources and explosive growth of the demand for LIBs may increase the production cost of LIBs and restrict their future availability; therefore, despite the undeniable advantages of LIBs, the development of alternative energy technologies is needed [8,14–18].

Recently, potassium-ion batteries (KIBs) have been reported as one of promising alternatives to LIBs owing to the abundant potassium resources in the earth and the lower standard redox potential of potassium relative to those of sodium and magnesium (K/K^+: −2.93 V *vs.* SHE; Na/Na^+: −2.71 V *vs.* SHE; Mg/Mg^{2+}: −2.27 V *vs.* SHE) [10,11,15,19–27]. Moreover, KIBs based on monovalent K^+ ion as a charge carrier exhibit intercalation chemistry, which is similar to LIBs that use monovalent Li^+ ion as a charge carrier [17,28]. More important is that K ions can be intercalated into the graphite, which is being adopted as commercial anodes for LIBs [10,29–32]. Thus, it is expected that KIBs can be the alternative of LIBs other than rechargeable battery systems [10,25,27,33]. However, because K^+ ions are larger than Li^+ ions (~1.38 Å vs. ~0.76 Å), K^+ ion diffusion into the host structure may be more sluggish

* Corresponding author.
** Corresponding author.
E-mail addresses: smyung@sejong.ac.kr (S.-T. Myung), jongsoonkim@sejong.ac.kr (J. Kim).
[1] These authors contributed equally to this work.

https://doi.org/10.1016/j.nanoen.2019.104184
Received 15 August 2019; Received in revised form 6 October 2019; Accepted 7 October 2019
Available online 10 October 2019

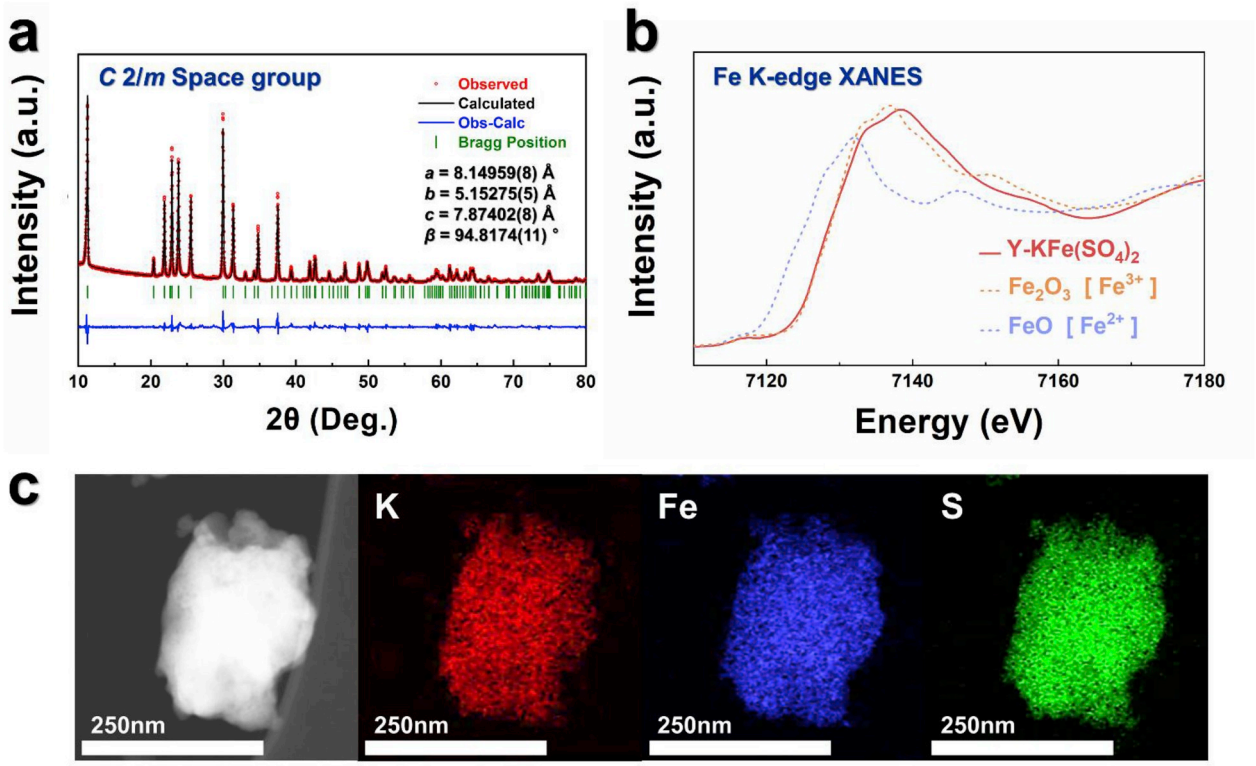

Fig. 1. (a) Rietveld refinement of XRD pattern of Y–$KFe(SO_4)_2$ ($R_P = 5.78\%$, $R_I = 4.49\%$, $R_F = 4.05\%$, $\chi^2 = 5.94\%$). (b) Fe K-edge XANES spectra of Y–$KFe(SO_4)_2$. (c) TEM–EDS map of Y–$KFe(SO_4)_2$ (atomic ratio of K:Fe = 1:1.08).

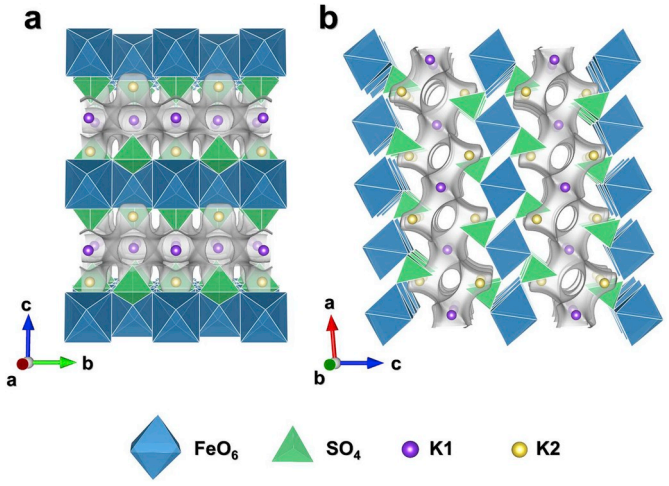

Fig. 2. (a), (b) BVS analyses of Y–$KFe(SO_4)_2$ with all possible K-ion sites in the crystal structure.

than Li^+ ion diffusion; in addition, K-ion intercalation is accompanied by a larger volume change during charge/discharge than Li-ion intercalation [10,34,35]. This issue necessitates to explore cathode materials with large ionic pathways in order to secure for facile K^+ diffusion. Similar to the case for LIBs, various layered-type materials utilizing oxygen as a connecting element have been studied as cathode materials for KIBs because of their high theoretical capacity and large two-dimensional ionic pathways [35–37]. However, the average operation voltage of most reported layered-type cathode materials for KIBs is less than 3.0 V (*vs.* K^+/K); in addition, these materials require a deep discharge process to 1.5 V (vs. K^+/K) to realize the large specific capacities. Three-dimensional structure materials supported by polyanions as the connecting elements instead of oxygen, such as $(XO_4)^{2-\text{ or }3-}$ (X = P, S, *etc.*) have inductive effect which can raise the redox potential of transition metal ions neighboring polyanions. In addition, the presence of strong covalent bond between X and O provides structural stability, so that the presences of the above polyanion in the structure prevent unwanted structural degradation during de/intercalation of K^+ ions with large ionic size [38–40].

Herein, we study the electrochemical and structural properties and the reaction mechanism on yavapaiite-type $KFe(SO_4)_2$ (Y–$KFe(SO_4)_2$) as a cathode material for KIBs. Although T. Masese et al. recently reported the preliminary studies on possibility of Y–$KFe(SO_4)_2$ as the cathode for KIBs [41], the detailed experiments and discussion on the structural and electrochemical properties on Y–$KFe(SO_4)_2$ should be required for the application of Y–$KFe(SO_4)_2$ as a cathode for KIBs. Through combination of first-principles calculation and various experimental techniques, we verify the physicochemical properties and reaction mechanism of Y–$KFe(SO_4)_2$ in a KIB system. Y–$KFe(SO_4)_2$ exhibits an average working voltage of ~3.3 V (*vs.* K^+/K) activated by an Fe^{3+}/Fe^{2+} redox reaction with a specific discharge capacity of 94 mAh g^{-1} at C/20 (1C = 94 mA g^{-1}), which approaches to its theoretical capacity. Even at 5C, the discharge capacity of Y–$KFe(SO_4)_2$ remains up to ~70% of its theoretical capacity, demonstrating the outstanding power capability of Y–$KFe(SO_4)_2$ as a promising cathode for KIBs. Moreover, the present Y–$KFe(SO_4)_2$ delivers excellent capacity retention of approximately 80% (*vs.* its initial capacity) for 300 cycles at 2C. For the first time, we report on the structure and the related electrochemical process for potassium ions storage in Y–$KFe(SO_4)_2$ that shows stable and long cycle life as a cathode materials for KIBs.

2. Results and discussion

The crystal structure of Y–$KFe(SO_4)_2$ was determined to be a

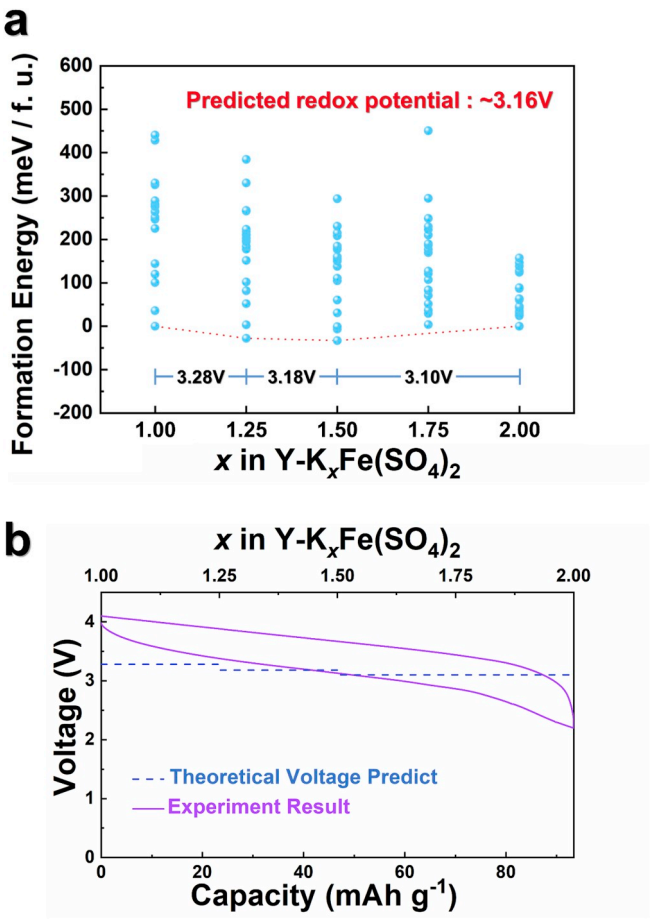

Fig. 3. (a) Formation energy of Y-$K_xFe(SO_4)_2$ ($1 \le x \le 2$) determined using convex hull method. (b) Charge/discharge profile of Y–$KFe(SO_4)_2$ in the voltage range of 4.1–2.2 V (*vs.* K^+/K).

yavapaiite-type structure with *C2/m* space group from Rietveld refinement of X-ray diffraction (XRD) data, and its lattice parameters were calculated to be $a = 8.14959$ (8) Å, $b = 5.15275$ (5) Å, and $c = 7.87402$ (8) Å (Fig. 1a). No impurities or second phases were detected in the XRD pattern, and the low R-factor confirms the accuracy of the Rietveld refinement ($R_P = 5.78\%$; $R_I = 4.49\%$; $R_F = 4.05\%$; $\chi^2 = 5.94\%$). Detailed structural information for Y–$KFe(SO_4)_2$, including the atomic positions, B_{iso}, and occupancies, is provided in Supporting Table T1. X-ray absorption near-edge structure (XANES) analysis indicated that the oxidation state of Fe ions in Y–$KFe(SO_4)_2$ was close to +3 (Fig. 1b). This result implies that additional alkali ions, such as K^+ ions, may be intercalated into the Y–$KFe(SO_4)_2$ structure through the Fe^{3+}/Fe^{2+} redox reaction, which is similar to the phenomenon observed in reported $Fe_2(SO_4)_3$ electrodes [20]. In addition, high-resolution transmission electron microscopy (HRTEM) combined with energy-dispersive X-ray spectroscopy (EDS) revealed that the primary particle size of Y–$KFe(SO_4)_2$ was below 100 nm in diameter and that the atomic ratio of K:Fe in Y–$KFe(SO_4)_2$ was approximately 1:1 (Fig. 1c) that is consistent with inductively coupled plasma atomic emission spectroscopy (ICP-AES) analysis (Supporting Table T2**)**. These results were also confirmed by scanning electron microscopy (SEM) analysis (Supporting Fig. S1).

To verify the availability of vacant sites for additional K^+ intercalation into the Y–$KFe(SO_4)_2$ structure, we performed bond-valance sum (BVS) analyses using the Bond_str program in the FullProf package [42,43]. Fig. 2a and b presents the crystal structure of Y–$KFe(SO_4)_2$ based on its structural information obtained from the Rietveld refinement shown in Fig. 1a. In the Y–$KFe(SO_4)_2$ framework, there are quasi-layers consisting of FeO_6 octahedra and SO_4 tetrahedra along the *ab* plane, which may result in the presence of large vacant sites for K^+ ions among the quasi-layers. It was predicted that there is one possible vacant site for additional K^+ intercalation into the Y–$KFe(SO_4)_2$ structure, with a Wyckoff position and atomic coordinates (*x*, *y*, *z*) of 4i and (0.25, 0.5, 0.25), respectively, indicating that an additional 2 mol K^+ ions per formula unit may theoretically be intercalated into the Y–$KFe(SO_4)_2$ structure. In addition, it is speculated that presence of sufficiently large diffusion pathways in the structure enables facile K^+ ion diffusion, implying the outstanding power-capability of Y–$KFe(SO_4)_2$ as a promising cathode for KIBs.

To understand the theoretical properties and reaction mechanism of Y-$K_xFe(SO_4)_2$ for K^+ intercalation, we performed first-principles calculations based on the structural information obtained from the Rietveld refinement and BVS analyses. Using cluster-assisted statistical mechanics (CASM) software, we prepared various K^+/vacancy configurations for Y-$K_xFe(SO_4)_2$ compositions ($1 \le x \le 2$). As shown in Fig. 3a, we arranged the formation energies of the various configurations of Y-$K_xFe(SO_4)_2$ and then calculated the theoretical redox potentials of Y-$K_xFe(SO_4)_2$ during K^+ de/intercalation using the following equation:

$$V = -\frac{E\left[K_{x_2}Fe(SO_4)_2\right] - E\left[K_{x_2}Fe(SO_4)_2\right] - (x_2 - x_1)E[K]}{(x_2 - x_1)F} \quad (1)$$

Here, *V* is the average redox potential of Y-$K_xFe(SO_4)_2$ in the compositional range of $x_1 \le x \le x_2$; *E* [$K_xFe(SO_4)_2$] represents the most stable energy of the various configurations of Y-$K_xFe(SO_4)_2$; *E*(K) is the energy of the K metal; and F is the Faraday constant. It was predicted that 1 mol of K^+ ions could be reversibly de/intercalated from/into the Y-$K_xFe(SO_4)_2$ structure in the available voltage ranges (*vs.* K^+/K). As shown in Fig. 3b, through comparison of the experimentally measured charge/discharge curve of Y-$K_xFe(SO_4)_2$ and its predicted redox potential based on the K^+ content ($1 \le x \le 2$), we confirmed that ~1 mol of K^+ ions can be intercalated into the Y-$K_xFe(SO_4)_2$ structure in the voltage range between 2.2 and 4.1 V (*vs.* K^+/K). In particular, the confirmed average operation voltage of Y-$K_xFe(SO_4)_2$ is ~3.3 V (*vs.* K^+/K), which is higher than that of reported Fe-based layered-type cathode materials for KIBs that highlights the 'inductive effect' enhanced by the presence of SO_4 moiety in the structure. Moreover, the sloppy charge/discharge curve of Y-$K_xFe(SO_4)_2$ corresponds well with the first-principles calculation data predicting the one-phase solid-solution reaction during K^+ de/intercalation. In addition, we performed the cyclic voltammogram (CV) analysis of Y–$KFe(SO_4)_2$ with the slow scanning rate of 5 μV s^{-1} in the voltage range of 2.2–4.1 V. As presented in Fig. S2, we observed one broad cathodic and anodic peaks in the CV curve of Y–$KFe(SO_4)_2$, unlike other layered-type cathode materials for KIBs. It was supposed that the reason why each voltage step is not clearly classified at CV curve of $KFe(SO_4)_2$ is due to very small gap among the voltage steps. Through first-principle calculation, we verified that the predicted redox potentials of Y–$K_{1+x}Fe(SO_4)_2$ for more than 0.25 mol K^+ intercalation are 3.1, 3.18 and 3.28 V (*vs.* K^+/K) and the voltage difference among them is just ~0.1 V, which is much smaller than the voltage difference among the predicted redox potentials of the other layered-type cathode materials [34,44].

The power-capability of electrode materials is known to greatly depend on the ionic mobility in the structure. Thus, to confirm the facile K^+ diffusion into the Y-$K_xFe(SO_4)_2$ structure, we performed nudged elastic band (NEB) calculations using first-principles calculations.

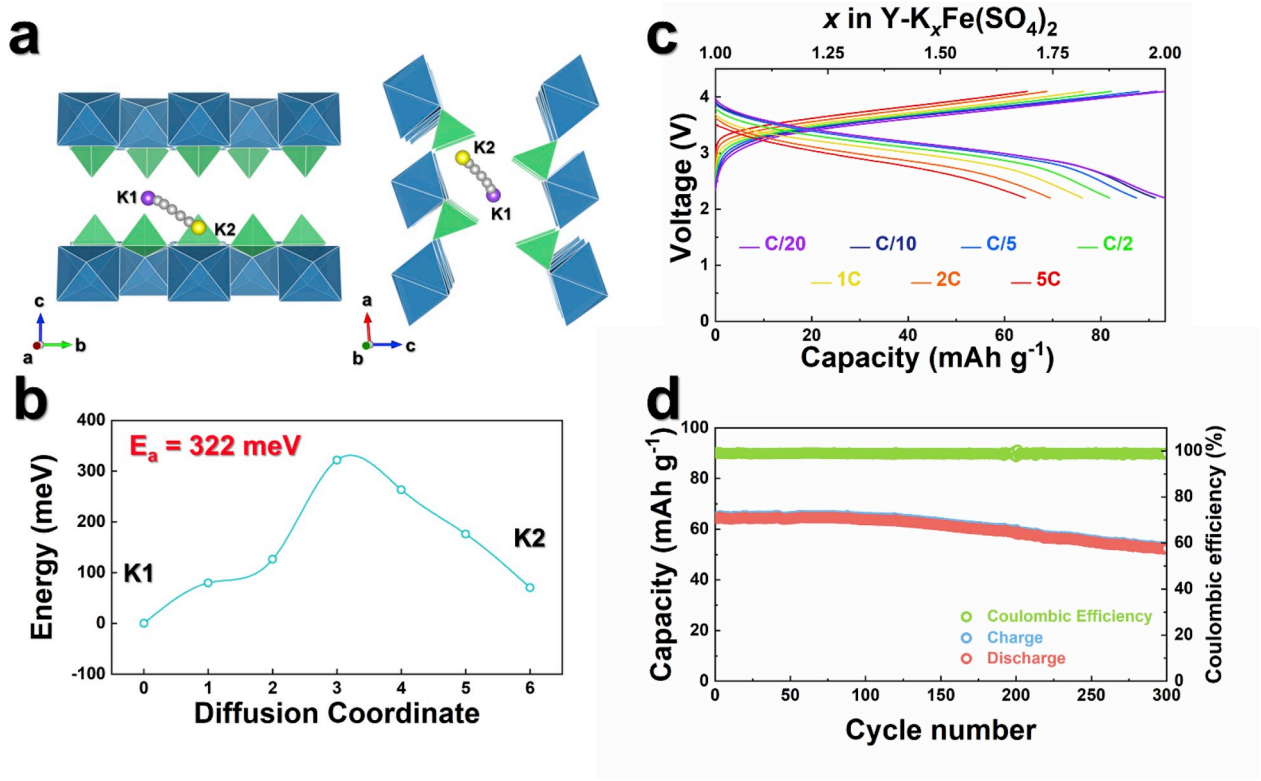

Fig. 4. (a) Visualized diffusion pathway and (b) activation energy plot of K1–K2 path in $KFe(SO_4)_2$ structure determined using NEB method. (c) Power capability of Y–$KFe(SO_4)_2$ at various C-rates. (d) Charge/discharge capacities and coulombic efficiency of Y–$KFe(SO_4)_2$ over 300 cycles at 2C.

Fig. 4a and b shows that the simulated activation barrier energy (E_a) required for K^+ diffusion along the pathways in the *ab* plane was only ~322 meV, which is sufficiently low for facile migration of K^+ ions in the structure. This calculation result suggests an outstanding power-capability of $KFe(SO_4)_2$ in the KIB system. As shown in Fig. 4c, we measured the specific capacities of Y-$K_xFe(SO_4)_2$ at various current rates (C/20, C/10, C/5, C/2, 1C, 2C, and 5C; 1C = 94 mA g^{-1}) in the voltage range between 2.2 and 4.1 V (*vs.* K^+/K). Interestingly, a high specific capacity of ~65 mAh g^{-1} was delivered at 5C, corresponding to ~70% of the theoretical capacity. Furthermore, the Y-$K_xFe(SO_4)_2$ retained approximately 80% of the initial capacity for 300 cycles at 2C, with a high Coulombic efficiency over 99% (Fig. 4d). It is thought that the good cyclability of Y-$K_xFe(SO_4)_2$ is related to the suggested simple structural variation during K^+ de/intercalation.

Operando/ex situ XRD analyses clearly confirmed that the Y-$K_xFe(SO_4)_2$ structure is continuously changed during discharge (Fig. 5a and b), indicating that Y-$K_xFe(SO_4)_2$ undergoes a single-phase reaction during K^+ intercalation. The positions of certain XRD peaks for Y-$K_xFe(SO_4)_2$, such as those of the (002), ($\bar{1}$11), ($\bar{2}$01), (111), ($\bar{1}$12), ($\bar{2}$02), and (112) peaks, slightly shifted during discharge, indicating the reversible K^+ intercalation into Y-$K_xFe(SO_4)_2$ without severe structural degradation (Fig. 5b). Although intensities of the (11n) peak get smaller during discharge, we can still detect the (11n) peak at the XRD pattern of $K_2Fe(SO_4)_2$ discharged to 2.2 V (*vs.* K^+/K). Moreover, we cannot observe any new XRD peaks indicating two-phase reaction at the XRD pattern, except the XRD peaks related to $KFe(SO_4)_2$. These results indicates the single-phase behavior of $K_{1+x}Fe(SO_4)_2$ during K^+ de/intercalation, which is similar with other electrode material based on the single-phase reaction [45,46]. Because of the large ionic size and monovalent property of K^+ ions, the existing K^+, Fe^{3+}, S^{6+} and O^{2-} ions in Y–$KFe(SO_4)_2$ are affected physically and chemically by the intercalated K^+ ions during discharge, which results in change of atomic positions of the existing ions in Y–$KFe(SO_4)_2$, and this structural change during K^+ intercalation can affect the XRD pattern. Thus, we supposed that decrease of the (11n) peak intensities during K^+ intercalation into Y–$KFe(SO_4)_2$ may result from change of atomic positions of existing ions in the structure. Furthermore, through Rietveld refinement of the *ex situ* XRD patterns, we calculated the change of the lattice parameters of Y-$K_xFe(SO_4)_2$ as a function of K content ($1 \leq x \leq 2$). As illustrated in Fig. 6a–d, the *a*, *b*, and *c* lattice parameters and volume of Y-$K_xFe(SO_4)_2$ simultaneously increased during K^+ intercalation. In particular, despite the large size of the K^+ ions, the volume change of Y-$K_xFe(SO_4)_2$ upon cycling was only ~1.83%, which is significantly smaller than that of other cathode materials for KIBs. It is thought that this small volume variation in volume is responsible for the outstanding cycle performance of the Y-$K_xFe(SO_4)_2$ cathode in the KIB system. In addition, the structural stability of Y-$K_xFe(SO_4)_2$ during repeated cycling was confirmed through XRD and TEM analyses. Supporting Fig. S3, and Supporting Table T3 show that the XRD patterns confirmed that there was negligible difference between the structure of the Y–$K_1Fe(SO_4)_2$ electrode after 300 cycles and that of the pristine Y–$K_1Fe(SO_4)_2$ electrode. Furthermore, the original particle shape of Y-$K_xFe(SO_4)_2$ and its atomic ratio were well retained without serious damage after 300 cycles. Supporting Fig. S4 and Supporting Table T4 shows the refined XRD pattern and structural information on fully potassiated Y–$K_2Fe(SO4)_2$. The Wyckoff position and atomic coordinate on the K2 site for newly intercalated K ions are 4i and (0.252, 0.5, 0.247), which is highly similar with the predicted atomic coordinate of the K2 site through BVS analyses. The atomic occupancy on the K2 site is approximately 0.5, which means the intercalation of 1 mol K^+ ions into Y–$KFe(SO_4)_2$ and formation of Y–$K_2Fe(SO4)_2$. Furthermore, we also

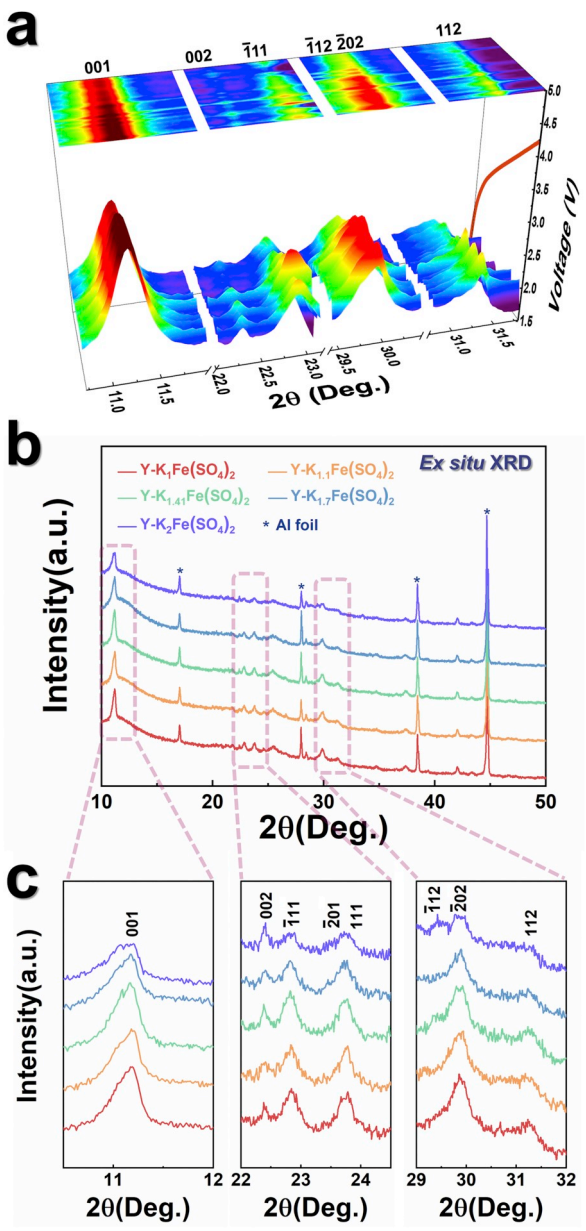

Fig. 5. (a) *Operando* XRD pattern of Y-$K_xFe(SO_4)_2$ ($1 \le x \le 2$). (b), (c) *Ex situ* XRD patterns of Y-$K_xFe(SO_4)_2$ ($1 \le x \le 2$).

confirmed that the Wyckoff position, atomic coordinate and atomic occupancy on the K1 site for original K ions in Y–$KFe(SO_4)_2$ were not changed despite the intercalation of 1 mol K^+ ions, which indicates the high stability of K^+ ions residing in the K1 site in Y–$KFe(SO_4)_2$. The low values of reliability factors ($R_P = 1.85\%$, $R_I = 3.41\%$, $R_F = 3.01\%$, $\chi^2 = 3.53\%$) exhibits high accuracy on our structural analyses using Rietveld refinement. In addition, through first-principles calculation, we confirmed that it is thermodynamically stable that all K ions in Y–$K_{1+x}Fe(SO_4)_2$ ($0 \le x \le 1$) are located at near (0, 0, 0.5) or (0.25, 0.5, 0.25), which is well consistent with the experimentally verified structural information on Y–$K_2Fe(SO4)_2$.

The reaction mechanism on Y-$K_xFe(SO_4)_2$ during charge/discharge was investigated through combined studies using *ex situ* XANES analyses and first-principles calculation. As presented in Fig. 7a, it was revealed that the Fe K-edge spectra of Y–$K_1Fe(SO_4)_2$ and Y–$K_2Fe(SO_4)_2$ were detected at the energy range similar with to those of Fe_2O_3 (Fe^{3+}) and FeO (Fe^{2+}), respectively. During discharge (or charge), the Fe K edge of Y-$K_xFe(SO_4)_2$ ($1 \le x \le 2$) continuously shifted toward lower (or higher) energy levels, indicating the Fe^{3+}/Fe^{2+} redox reaction. Furthermore, we predicted the integrated spin moments of Y–$K_1Fe(SO_4)_2$ and Y–$K_2Fe(SO_4)_2$ using first-principles calculation (Fig. 7b). During 1 mol K^+ intercalation into Y–$K_1Fe(SO_4)_2$, the equivalent amount of electrons are interacted with the 3*d* orbitals at the same time. Thus, total electron spin counts of Fe ions in Y-$K_xFe(SO_4)_2$ were changed from +5 to +4, implying Fe^{3+}/Fe^{2+} redox reaction. These results demonstrated that during charge/discharge, through the Fe^{3+}/Fe^{2+} redox reaction, 1 mol of K^+ ions can be stored in/extracted from Y-$K_xFe(SO_4)_2$.

3. Experimental

3.1. Synthesis process

Y–$KFe(SO_4)_2$ was prepared using low-temperature synthesis. K_2SO_4 and $Fe_2(SO_4)_3$ with a molar ratio of 1:1 were used as precursors. The precursors were fully dissolved in distilled water and placed on a hot plate for evaporation at 80 °C. After evaporation, the remaining yellow material was ground to produce a fine powder, which was then calcined at 200 °C for 4 h. After calcination, the color of the powder changed from yellow to light ivory.

3.2. Materials characterization

The structure of Y–$KFe(SO_4)_2$ was analyzed using an X-ray diffractometer (PANalytical, Empyrean) equipped with Cu Kα radiation ($\lambda = 1.54178$ Å). Structure data were collected over the 2θ range of 10°–80° with a step size of 0.01°. The microstructures of the samples were examined using SEM (HITACHI S-4700) with an accelerating voltage of 15 kV and transmission electron microscopy (TEM; JEM-F200) at accelerating voltages of 80 and 120 kV, respectively; in addition, elemental mapping was performed using EDS. Fe K-edge X-ray absorption spectra (XAS) profiles were obtained at beamline 7D at Pohang Accelerator Laboratory (PAL) using Fe metal foil as a reference. Operando XRD pattern was used to investigate the structural evolution during discharging at the 3D XRS beamline at PAL.

3.3. Electrochemical characterization

Electrochemical characterization was performed using a 2032-type coin cell assembled in an Ar-filled glovebox. Bare Y–$KFe(SO_4)_2$ and Super P carbon black were mixed in a weight ratio of 8:2 using high-energy ball milling at 150 rpm; the ball-milling jar was filled with Ar. To prepare the electrode, a slurry was prepared using the ball-milled powder, Super P carbon black, and polyvinylidene fluoride (PVDF) in a weight ratio of 8:1:1, and this mixture was dispersed in N-methyl-2-pyrrolidone (NMP). The slurry was applied onto Al foil to a thickness of 80 μm and dried in a vacuum oven at 100 °C. The dried electrode was punched into disks of 10π-mm diameter. The mass loading of the active material was 3×10^{-3} g cm^{-2}. The coin cell was assembled as a half-cell using K metal as the counter electrode, Whatman GF/F glass fiber as the separator, and 0.5 M KPF_6 in a 1:1:0.05 v/v mixture of ethylene carbonate (EC), propylene carbonate (PC), and fluoroethylene carbonate (FEC) as the electrolyte. Galvanostatic charge/discharge tests were performed at various C-rates (C/20, C/10, C/5, C/2, 1C, 2C, and 5C in the voltage range of 4.1–2.2 V; 1C is 94 mA g^{-1}) for $KFe(SO_4)_2$ using an automatic battery charge/discharge test system (WBCS 3000, WonATech).

3.4. Computational details

All the density functional theory (DFT) calculations were performed using the Vienna Ab initio Simulation Package (VASP) [40]. We used projector-augmented wave (PAW) pseudopotentials [47] with a plane-wave basis set as implemented in VASP.

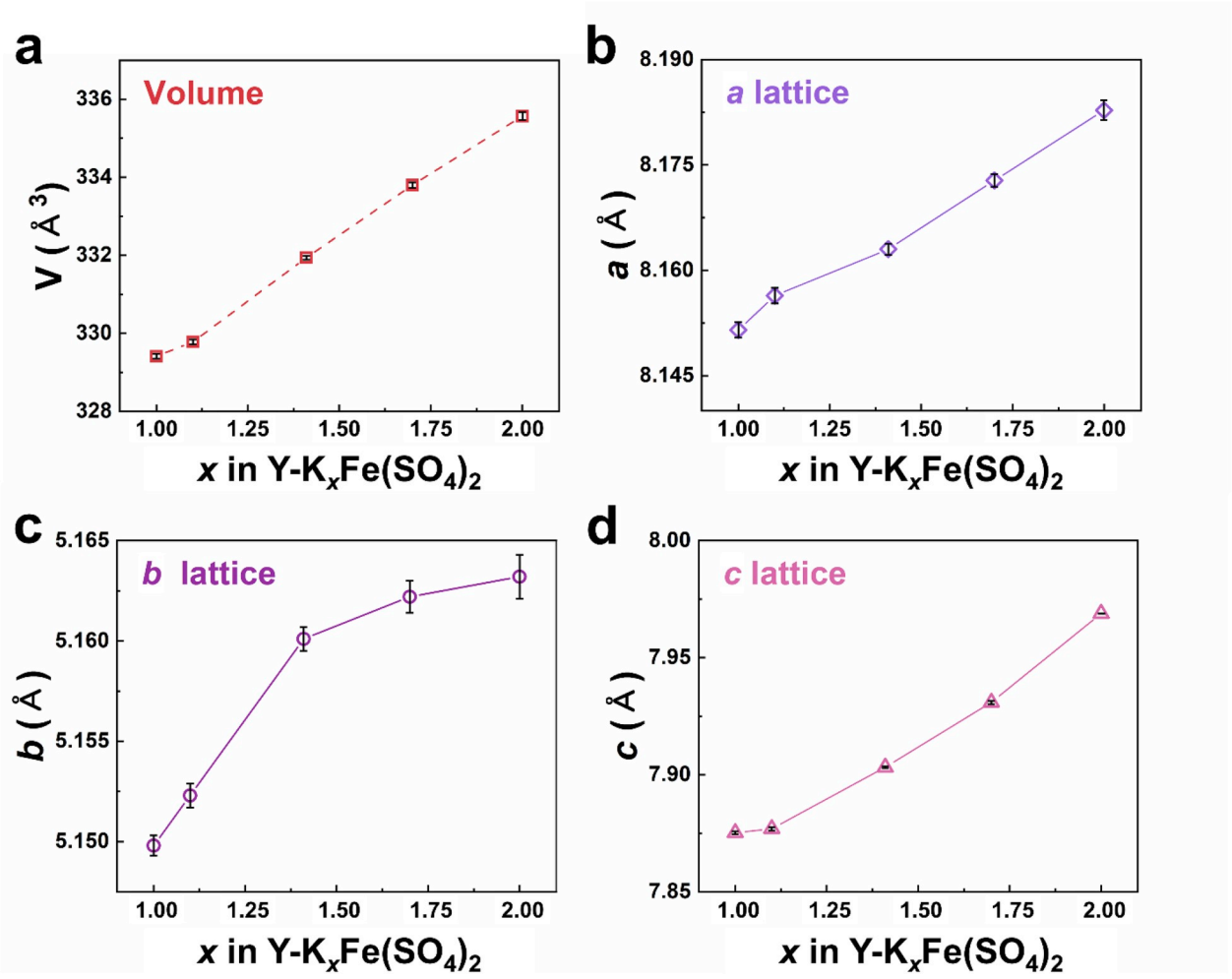

Fig. 6. Change in (a) volume, (b) lattice parameter *a*, (c) lattice parameter *b*, and (d) lattice parameter *c* of Y-$K_xFe(SO_4)_2$ ($1 \leq x \leq 2$) (error bars, black).

Perdew–Burke–Ernzerhof (PBE) parametrization of the generalized gradient approximation (GGA) [48] was used for the exchange-correlation functional. For the DFT calculations, a $3 \times 3 \times 2$ k-point grid was used to calculate a $1 \times 1 \times 1$ supercell structure of $KFe(SO_4)_2$. The GGA + U method [49] was adopted to address the localization of the d-orbital in Fe ions using a U value of 4.3 eV, which was used in a previous study on $NaFePO_4$ [50]. An appropriate number of k-points and a kinetic energy cutoff of 500 eV were used in all the calculations. All the structures were optimized until the force in the unit cell converged to within 0.05 eV $Å^{-1}$.

CASM software [51] was used to generate all the K/vacancy configurations for each composition, followed by full DFT calculations on a maximum of 20 configurations with the lowest electrostatic energy for each composition used to obtain the convex hull of Y–$KFe(SO_4)_2$ for KIBs.

NEB calculations [52] were performed to determine the activation barrier for Na diffusion in the theoretical Y–$K_2Fe(SO_4)_2$ structure. A $1 \times 2 \times 1$ supercell was adapted to avoid the interactions between periodic unit cells. To perform the calculations, five intermediate images were generated between each K site. These structures were then calculated using a NEB algorithm with fixed lattice parameters and free internal atomic positions.

4. Conclusion

We successfully demonstrated the potential of Y–$KFe(SO_4)_2$ as a promising cathode material for KIBs for the first time. The availability of sufficient diffusion paths for K ions in the Y–$KFe(SO_4)_2$ structure was verified through Rietveld refinement and BVS analysis based on XRD patterns. Using first-principles calculations, Y–$KFe(SO_4)_2$ was predicted to have excellent power capability and a high average voltage. In electrochemical tests, Y–$KFe(SO_4)_2$ delivered a discharge capacity of 94 mAh g^{-1} at C/20 in the voltage range of 4.1–2.2 V, with an average working voltage of ~3.3 V. In addition, a capacity of ~70 mAh g^{-1} was retained at 5C, corresponding to capacity retention of ~70%. Furthermore, the capacity retention of $KFe(SO_4)_2$ at 2C was approximately 80% of the initial capacity after 300 cycles, with a Coulombic efficiency of over 99%.This outstanding performance was attributed to the reversible Fe^{2+}/Fe^{3+} oxidation in Y–$KFe(SO_4)_2$ and the small volume change of 1.83% during charge and discharge despite the large ionic radius of the KIB system. Our findings demonstrate the great potential of Y–$KFe(SO_4)_2$ as a cathode material for KIBs and provide insight for the development and improvement of new cathode materials for KIBs.

Declaration of Competing Interest

The authors declare that they have no known competing financial interests or personal relationships that could have appeared to influence the work reported in this paper.

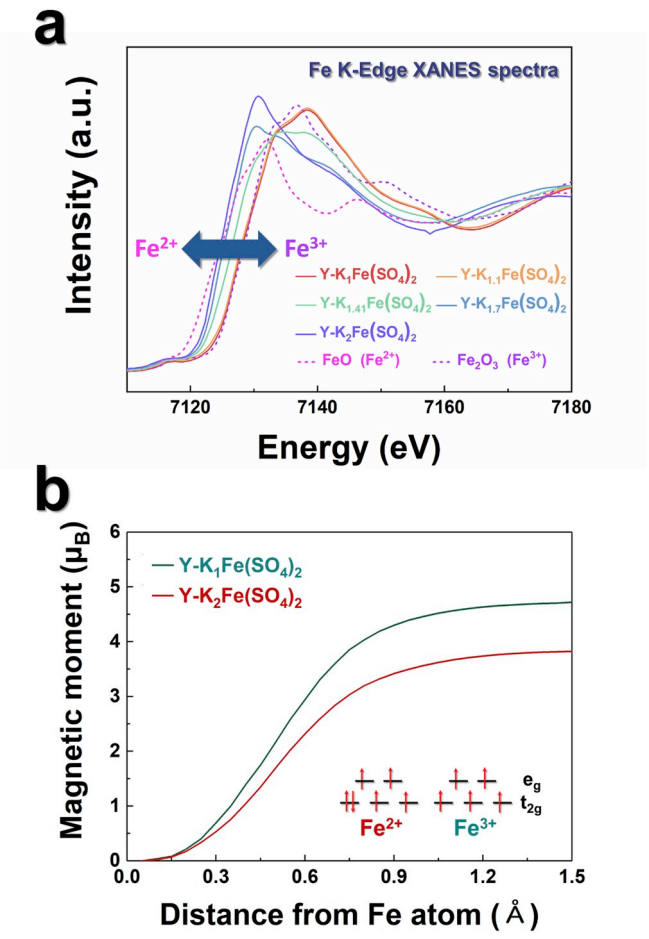

Fig. 7. (a) *Ex situ* analyses of Y-$K_xFe(SO_4)_2$ ($1 \leq x \leq 2$) Fe K-edge XANES spectra. (b) the integrated spin moments of Y–$K_1Fe(SO_4)_2$ (=Fe^{3+}) and Y–$K_2Fe(SO_4)_2$ (=Fe^{2+}).

Acknowledgment

This research was supported by the Radiation Technology R&D program of the National Research Foundation of Korea funded by the Ministry of Science and ICT of Korea (NRF-2017M2A2A6A01070834, NRF-2019M2A2A6A05102365), International Research & Development Program of the National Research Foundation of Korea funded by the Ministry of Science and ICT of Korea (NRF-2018K2A9A2A12000230), General Research Program of the National Research Foundation of Korea funded by the Ministry of Science and ICT of Korea (NRF-2019R1F1A1063415), and Global Research Development Center (GRDC) program of the National Research Foundation of Korea funded by the Ministry of Science and ICT of Korea (NRF-2018K1A4A3A01064272).

Appendix A. Supplementary data

Supplementary data to this article can be found online at https://doi.org/10.1016/j.nanoen.2019.104184.

References

[1] J. Kim, H. Kim, I. Park, Y.U. Park, J.K. Yoo, K.Y. Park, S. Lee, K. Kang, $LiFePO_4$ with an alluaudite crystal structure for lithium ion batteries, Energy Environ. Sci. 6 (2013) 830–834, https://doi.org/10.1039/c3ee24393a.
[2] K. Kang, Electrodes with high power and high capacity for rechargeable lithium batteries, Science 311 (2006) 977–980, https://doi.org/10.1126/science.1122152.
[3] J.B. Goodenough, K.S. Park, The Li-ion rechargeable battery: a perspective, J. Am. Chem. Soc. 135 (2013) 1167–1176, https://doi.org/10.1021/ja3091438.
[4] G. Peng, X. Yao, H. Wan, B. Huang, J. Yin, F. Ding, X. Xu, Insights on the fundamental lithium storage behavior of all-solid-state lithium batteries containing the $LiNi_{0.8}Co_{0.15}Al_{0.05}O_2$ cathode and sulfide electrolyte, J. Power Sources 307 (2016) 724–730, https://doi.org/10.1016/j.jpowsour.2016.01.039.
[5] B.C. Melot, J.M. Tarascon, Design and preparation of materials for advanced electrochemical storage, Acc. Chem. Res. 46 (2013) 1226–1238, https://doi.org/10.1021/ar300088q.
[6] M. Armand, J.-M. Tarascon, Building better batteries, Nature 451 (2008) 652–657, https://doi.org/10.1038/451652a.
[7] H. Kim, H. Kim, Z. Ding, M.H. Lee, K. Lim, G. Yoon, K. Kang, Recent progress in electrode materials for sodium-ion batteries, Adv. Energy Mater. 6 (2016) 1–38, https://doi.org/10.1002/aenm.201600943.
[8] S.W. Kim, D.H. Seo, X. Ma, G. Ceder, K. Kang, Electrode materials for rechargeable sodium-ion batteries: potential alternatives to current lithium-ion batteries, Adv. Energy Mater. 2 (2012) 710–721, https://doi.org/10.1002/aenm.201200026.
[9] J. Kim, H. Kim, S. Lee, S.T. Myung, Development of a new alluaudite-based cathode material with high power and long cyclability for application in Na ion batteries in real-life, J. Mater. Chem. A. 5 (2017) 22334–22340, https://doi.org/10.1039/c7ta06693g.
[10] Y. Marcus, Thermodynamic functions of transfer of single ions from water to nonaqueous and mixed solvents: Part 3 - standard potentials of selected electrodes, Pure Appl. Chem. 57 (2007) 1129–1132, https://doi.org/10.1351/pac198557081129.
[11] C.H. Jo, J.U. Choi, H. Yashiro, S.T. Myung, Controllable charge capacity using a black additive for high-energy-density sodium-ion batteries, J. Mater. Chem. A. 7 (2019) 3903–3909, https://doi.org/10.1039/c8ta09833f.
[12] R. Wang, G. Qian, T. Liu, M. Li, J. Liu, B. Zhang, W. Zhu, S. Li, W. Zhao, W. Yang, X. Ma, Z. Fu, Y. Liu, J. Yang, L. Jin, Y. Xiao, F. Pan, Tuning Li-enrichment in high-Ni layered oxide cathodes to optimize electrochemical performance for Li-ion battery, Nano Energy 62 (2019) 709–717, https://doi.org/10.1016/j.nanoen.2019.05.089.
[13] Y. Liu, L. Tang, H. Wei, X. Zhang, Z. He, Y. Li, J. Zheng, Enhancement on structural stability of Ni-rich cathode materials by in-situ fabricating dual-modified layer for lithium-ion batteries, Nano Energy 65 (2019) 104043, https://doi.org/10.1016/j.nanoen.2019.104043.
[14] J. Kim, I. Park, H. Kim, K.Y. Park, Y.U. Park, K. Kang, Tailoring a new 4V-class cathode material for Na-ion batteries, Adv. Energy Mater. 6 (2016) 6–9, https://doi.org/10.1002/aenm.201502147.
[15] R.A. Shakoor, D.H. Seo, H. Kim, Y.U. Park, J. Kim, S.W. Kim, H. Gwon, S. Lee, K. Kang, A combined first principles and experimental study on $Na_3V_2(PO_4)_2F_3$ for rechargeable Na batteries, J. Mater. Chem. 22 (2012) 20535–20541, https://doi.org/10.1039/c2jm33862a.
[16] K.T. Kim, C.Y. Yu, C.S. Yoon, S.J. Kim, Y.K. Sun, S.T. Myung, Carbon-coated $Li_4Ti_5O_{12}$ nanowires showing high rate capability as an anode material for rechargeable sodium batteries, Nano Energy 12 (2015) 725–734, https://doi.org/10.1016/j.nanoen.2015.01.034.
[17] Y. Liu, Z. Tai, Q. Zhang, H. Wang, W.K. Pang, H.K. Liu, K. Konstantinov, Z. Guo, A new energy storage system: rechargeable potassium-selenium battery, Nano Energy 35 (2017) 36–43, https://doi.org/10.1016/j.nanoen.2017.03.029.
[18] W. Hong, Y. Zhang, L. Yang, Y. Tian, P. Ge, J. Hu, W. Wei, G. Zou, H. Hou, X. Ji, Carbon quantum dot micelles tailored hollow carbon anode for fast potassium and sodium storage, Nano Energy 65 (2019) 104038, https://doi.org/10.1016/j.nanoen.2019.104038.
[19] J.H. Jo, J.-Y. Hwang, J.U. Choi, H.J. Kim, Y.-K. Sun, S.-T. Myung, Potassium vanadate as a new cathode material for potassium-ion batteries, J. Power Sources 432 (2019) 24–29, https://doi.org/10.1016/j.jpowsour.2019.05.064.
[20] F. Meirer, C. Streli, G. Pepponi, P. Wobrauschek, M.A. Zaitz, C. Horntrich, G. Falkenberg, Feasibility study of SR-TXRF-XANES analysis for iron contaminations on a silicon wafer surface, Surf. Interface Anal. 40 (2008) 1571–1576, https://doi.org/10.1002/sia.2954.
[21] Z. Jian, W. Luo, X. Ji, Carbon electrodes for K-ion batteries, J. Am. Chem. Soc. 137 (2015) 11566–11569, https://doi.org/10.1021/jacs.5b06809.
[22] V. Palomares, M. Casas-Cabanas, E. Castillo-Martínez, M.H. Han, T. Rojo, Update on Na-based battery materials. A growing research path, Energy Environ. Sci. 6 (2013) 2312–2337, https://doi.org/10.1039/c3ee41031e.
[23] B.L. Ellis, W.R.M. Makahnouk, Y. Makimura, K. Toghill, L.F. Nazar, A multifunctional 3.5V iron-based phosphate cathode for rechargeable batteries, Nat. Mater. 6 (2007) 749–753, https://doi.org/10.1038/nmat2007.
[24] Q. Yang, Z. Wang, W. Xi, G. He, Tailoring nanoporous structures of Ge anodes for stable potassium-ion batteries, Electrochem. Commun. 101 (2019) 68–72, https://doi.org/10.1016/J.ELECOM.2019.02.016.
[25] J.C. Pramudita, D. Sehrawat, D. Goonetilleke, N. Sharma, An initial review of the status of electrode materials for potassium-ion batteries, Adv. Energy Mater. 7 (2017) 1–21, https://doi.org/10.1002/aenm.201602911.
[26] J. Kim, H. Kim, S. Lee, High power cathode material $Na_4VO(PO_4)_2$with open framework for Na ion batteries, Chem. Mater. 29 (2017) 3363–3366, https://doi.org/10.1021/acs.chemmater.6b04557.
[27] X.H. Zhang, W.L. Pang, F. Wan, J.Z. Guo, H.Y. Lü, J.Y. Li, Y.M. Xing, J.P. Zhang, X. L. Wu, P2-$Na_{2/3}Ni_{1/3}Mn_{5/9}Al_{1/9}O_2$ microparticles as superior cathode material for sodium-ion batteries: enhanced properties and mechanisam via graphene connection, ACS Appl. Mater. Interfaces 8 (2016) 20650–20659, https://doi.org/10.1021/acsami.6b03944.
[28] W. Zhang, Z. Wu, J. Zhang, G. Liu, N.H. Yang, R.S. Liu, W.K. Pang, W. Li, Z. Guo, Unraveling the effect of salt chemistry on long-durability high-phosphorus-concentration anode for potassium ion batteries, Nano Energy 53 (2018) 967–974, https://doi.org/10.1016/j.nanoen.2018.09.058.

[29] A. Metrot, D. Guerard, D. Billaud, A. Herold, New results about the sodium-graphite system, Synth. Met. 1 (1980) 363–369, https://doi.org/10.1016/0379-6779(80)90071-5.
[30] N. Adhoum, J. Bouteillon, D. Dumas, J.C. Poignet, Electrochemical insertion of sodium into graphite in molten sodium fluoride at 1025 °C, Electrochim. Acta 51 (2006) 5402–5406, https://doi.org/10.1016/j.electacta.2006.02.019.
[31] M. Fouletier, G. Pascal, Electrochemical intercalation of graphite into sodium, Solid State Ion. 30 (1988) 1172–1175, https://doi.org/10.1016/0167-2738(88)90351-7.
[32] J.U. Choi, J. Kim, J.-Y. Hwang, J.H. Jo, Y.-K. Sun, S.-T. Myung, $K_{0.54}[Co_{0.5}Mn_{0.5}]O_2$: new cathode with high power capability for potassium-ion batteries, Nano Energy 61 (2019) 284–294, https://doi.org/10.1016/j.nanoen.2019.04.062.
[33] L. Zhang, B. Zhang, C. Wang, Y. Dou, Q. Zhang, Y. Liu, H. Gao, M. Al-Mamun, W. K. Pang, Z. Guo, S.X. Dou, H.K. Liu, Constructing the best symmetric full K-ion battery with the NASICON-type K 3 V 2 (PO 4) 3, Nano Energy 60 (2019) 432–439, https://doi.org/10.1016/j.nanoen.2019.03.085.
[34] J.Y. Hwang, J. Kim, T.Y. Yu, S.T. Myung, Y.K. Sun, Development of P3-$K_{0.69}CrO_2$ as an ultra-high-performance cathode material for K-ion batteries, Energy Environ. Sci. 11 (2018) 2821–2827, https://doi.org/10.1039/c8ee01365a.
[35] S. Komaba, T. Hasegawa, M. Dahbi, K. Kubota, Potassium intercalation into graphite to realize high-voltage/high-power potassium-ion batteries and potassium-ion capacitors, Electrochem. Commun. 60 (2015) 172–175, https://doi.org/10.1016/j.elecom.2015.09.002.
[36] W. Ko, T. Park, H. Park, Y. Lee, K.E. Lee, J. Kim, $Na_{0.97}KFe(SO_4)_2$: an iron-based sulfate cathode material with outstanding cyclability and power capability for Na-ion batteries, J. Mater. Chem. A. 6 (2018) 17095–17100, https://doi.org/10.1039/c8ta05854g.
[37] Y. Li, C. Yang, F. Zheng, Q. Pan, Y. Liu, G. Wang, T. Liu, J. Hu, M. Liu, Design of TiO_2eC hierarchical tubular heterostructures for high performance potassium ion batteries, Nano Energy 59 (2019) 582–590, https://doi.org/10.1016/j.nanoen.2019.03.002.
[38] C. Liu, Z.G. Neale, G. Cao, Understanding electrochemical potentials of cathode materials in rechargeable batteries, Mater. Today 19 (2016) 109–123, https://doi.org/10.1016/j.mattod.2015.10.009.
[39] P. Barpanda, G. Oyama, S.I. Nishimura, S.C. Chung, A. Yamada, A 3.8-V earth-abundant sodium battery electrode, Nat. Commun. 5 (2014) 1–8, https://doi.org/10.1038/ncomms5358.
[40] H. He, D. Huang, Y. Tang, Q. Wang, X. Ji, H. Wang, Z. Guo, Tuning nitrogen species in three-dimensional porous carbon via phosphorus doping for ultra-fast potassium storage, Nano Energy 57 (2019) 728–736, https://doi.org/10.1016/j.nanoen.2019.01.009.
[41] T. Masese, K. Yoshii, Y. Yamaguchi, T. Okumura, Z.D. Huang, M. Kato, K. Kubota, J. Furutani, Y. Orikasa, H. Senoh, H. Sakaebe, M. Shikano, Rechargeable potassium-ion batteries with honeycomb-layered tellurates as high voltage cathodes and fast potassium-ion conductors, Nat. Commun. 9 (2018) 1–12, https://doi.org/10.1038/s41467-018-06343-6.
[42] J. Rodríguez-Carvajal, Recent developments of the program FULLPROF, Comm. Powder Diffr. (IUCr). Newsl. 26 (2001) 12–19.
[43] S. Adams, Modelling ion conduction pathways by bond valence pseudopotential maps, Solid State Ion. 136–137 (2000) 1351–1361, https://doi.org/10.1016/S0167-2738(00)00576-2.
[44] H. Kim, D.H. Seo, J.C. Kim, S.H. Bo, L. Liu, T. Shi, G. Ceder, Investigation of potassium storage in layered P3-type K0.5MnO2 cathode, Adv. Mater. 29 (2017) 1–6, https://doi.org/10.1002/adma.201702480.
[45] D. Shimizu, S.I. Nishimura, P. Barpanda, A. Yamada, Electrochemical redox mechanism in 3.5 V $Li_{2-x}FeP_2O_7$ ($0 \leq x \leq 1$) pyrophosphate cathode, Chem. Mater. 24 (2012) 2598–2603, https://doi.org/10.1021/cm301337z.
[46] H. Kim, I. Park, S. Lee, H. Kim, K.Y. Park, Y.U. Park, H. Kim, J. Kim, H.D. Lim, W. S. Yoon, K. Kang, Understanding the electrochemical mechanism of the new iron-based mixed-phosphate $Na_4Fe_3(PO_4)_2(P_2O_7)$ in a Na rechargeable battery, Chem. Mater. 25 (2013) 3614–3622, https://doi.org/10.1021/cm4013816.
[47] P.E. Blöchl, Projector augmented-wave method, Phys. Rev. B. 50 (1994) 17953–17979, https://doi.org/10.1103/PhysRevB.50.17953.
[48] J.P. Perdew, K. Burke, M. Ernzerhof, Generalized gradient approximation made simple, Phys. Rev. Lett. 77 (1996) 3865–3868, https://doi.org/10.1103/PhysRevLett.77.3865.
[49] V.I. Anisimov, F. Aryasetiawan, A.I. Lichtenstein, First-principles calculations of the electronic structure and spectra of strongly correlated systems: the LDA + U method, J. Phys. Condens. Matter 9 (1997) 767–808, https://doi.org/10.1088/0953-8984/9/4/002.
[50] J. Kim, D.H. Seo, H. Kim, I. Park, J.K. Yoo, S.K. Jung, Y.U. Park, W.A. Goddard, K. Kang, Unexpected discovery of low-cost maricite NaFePO4 as a high-performance electrode for Na-ion batteries, Energy Environ. Sci. 8 (2015) 540–545, https://doi.org/10.1039/c4ee03215b.
[51] A. Van der Ven, J.C. Thomas, Q. Xu, J. Bhattacharya, Linking the electronic structure of solids to their thermodynamic and kinetic properties, Math. Comput. Simulat. 80 (2010) 1393–1410, https://doi.org/10.1016/J.MATCOM.2009.08.008.
[52] G. Henkelman, B.P. Uberuaga, H. Jónsson, A climbing image nudged elastic band method for finding saddle points and minimum energy paths, J. Chem. Phys. 113 (2000) 9901–9904, https://doi.org/10.1063/1.1329672.